# AN ANALTICAL MODEL FOR VIBRATION ANALYSIS OF DISK RESONATOR GYROSCOPES

*Mehran Hosseini-Pishrobat[1], Baha Erim Uzunoglu[1], Derin Erkan[1], and Erdinc Tatar[1,2]*
[1]Department of Electrical and Electronics Engineering, Bilkent University, Ankara, Turkey
[2]National Nanotechnology Research Center (UNAM), Bilkent University, Ankara, Turkey

2022 IEEE International Symposium on Inertial Sensors and Systems (INERTIAL) | 978-1-6654-0282-8/22/$31.00 ©2022 IEEE | DOI: 10.1109/INERTIAL53425.2022.9787727

## ABSTRACT

Disk resonator gyroscopes (DRGs) utilize the circular symmetry of a set of concentric rings to realize high-performance MEMS gyroscopes. We set forth an analytical method to calculate the mode shapes of the rings and then obtain the corresponding modal mass, Coriolis mass, and stiffness. Following the Ritz method, we minimize the total potential energy of the rings subject to the boundary conditions imposed by the spokes that connect the rings. We show the efficacy of our method using the frequency response of a fabricated DRG and comparison with the finite element method (FEM). With respect to the FEM, our modeling is more straightforward, more intuitive, and can be extended to model imperfections and ensuing effects such as quadrature error and frequency split.

## KEYWORDS

Disk resonator gyroscope, MEMS, Mode shape, the Ritz method

## INTRODUCTION

DRGs are Coriolis-based gyroscopes that can operate at either angular rate or whole angle modes [1]. The circular symmetry of disks and rings endows the gyroscope's structure with pairs of frequency-matched mode shapes. This property, along with the advantages such as high thermal stability, high quality factor, and shock resistance, puts DRGs forward as a promising candidate for high-performance MEMS gyroscopes [2], [3]. Mathematical modeling of single or double ring-based gyroscopes has been studied in the literature; see, for example, [4], [5]. However, there are a few works on the modeling of multi-ring DRGs. For mode shape calculation and lumped parameter modeling of DRGs, Li et al. [6] used the component mode synthesis method, and Lin et al. [7] adopted the ray tracing method from the wave propagation theory.

Our main contribution is to present a new analytical model for calculating the vibrational properties of disk resonator gyroscopes (DRGs) with a multi-ring structure. Given the mode shapes of the outermost ring (e.g., the wine glass modes), we formulate the boundary conditions at the interconnection of the rings by spokes and parameterize the mode shapes of the inner rings in terms of suitable basis functions. Following the Ritz method, we solve a least-squares optimization problem to calculate the mode shapes and then obtain the corresponding modal mass, Coriolis mass, and stiffness. We assess our method with the experimental data of a (111) Si, $\cos(2\theta)$ DRG, which was designed by our group, and its fabrication was outsourced [8]; Figure 1-(a) shows the SEM image of the device. Compared to the commonly used FEM, our modeling is more intuitive and computationally simpler. The advantages of our method over the existing ones in [6], [7] are its simplicity and computational efficiency. Moreover, we present our method in a general setting for the $n$-th mode of the rings, so it can be used for a $\cos(3\theta)$ device. Additionally, our approach is capable of handling the geometrical/material imperfections in its formulation.

*Notation:* $[.]^{\mathsf{T}}$ and $\otimes$ stand for matrix transpose and Kronecker product, respectively. $\mathrm{diag}(x_i)_{i=n_1}^{n_2}$ $(n_2 \geq n_1)$ is the diagonal matrix with the diagonal entries $x_{n_1}, \dots, x_{n_2}$.

## MATHEMATICAL MODELING OF DRG

As shown in Figure 1-(c), the core mechanical structure of our DRG consists of $N_r$ concentric rings, numbered consecutively from outside to inside as Ring#1, Ring#2, …, and Ring#$N_r$. We use the polar coordinates $(r, \theta)$ to study the in-plane vibration of the rings. We denote by $R_i$, $w_i$, $A_i$, and $I_i$ the mean radius, width, cross-section area, and second moment of the cross-section area of Ring#$i$, respectively. We assume the rings to be thin (i.e., $\frac{w_i}{R_i} \ll 1$), inextensible, and governed by the Euler-Bernoulli beam theory. For $i = 1{:}\,N_r - 1$, Ring#$i$ and Ring#$i+1$ are connected by $4n$ beams—referred as the *spokes*—that are located at the angles $\theta_{i,j}$, $j = 1{:}\,4n$, and each have the length $\ell$; here, $n \geq 2$ is the mode number for the operation of the device that we will discuss shortly. The angular positions of the spokes alternate between two configurations with $\pi/4n$ relative angle shift; more specifically,

$$\theta_{i,j} = \begin{cases} \frac{\pi}{2n}(j-1) \text{ if } i \text{ is odd}, \\ \frac{\pi}{4n}(2j-1) \text{ if } i \text{ is even}, \end{cases} \quad (1)$$

where $j = 1{:}\,4n$. The last set of spokes connects Ring#$N_r$ to a rigid anchored disk. We note that Ring#1 is the main vibrating component that we electrostatically drive into resonance and detect its motion; the rest of the rings along with the spokes have the role of a supporting suspension system for Ring#1. We denote by $u_{r,i}(\theta, t)$ and $u_{\theta,i}(\theta, t)$ the radial and tangential components of the displacement field of Ring#$i$, respectively, where $t \geq 0$ is time.

### Boundary conditions

We consider the spokes, because of their large width-to-length ratio, as rigid connections. This, in turn, implies the following set of boundary conditions:

*Radial motion:* At the connection points, because of the axial rigidity of the spokes, Ring#$i$ and Ring#$i+1$, $i = 1{:}\,N_r - 1$, have the same radial displacements, and Ring#$N_r$ has zero radial displacement because of its connection to the anchored disk:

$$u_{r,i+1}(\theta_{i,j}, t) = u_{r,i}(\theta_{i,j}, t), i = 1{:}\,N_r - 1, j = 1{:}\,4n, \quad (2)$$
$$u_{r,N_r}(\theta_{N_r,j}, t) = 0, j = 1{:}\,4n.$$

*Tangential motion:* the $j$-th spoke rigidly transmits the tangential displacement of Ring#$i$ to Ring#$i+1$, which then generates a tangential displacement and a local rotation at Ring#$i+1$. This rotation is the superposition

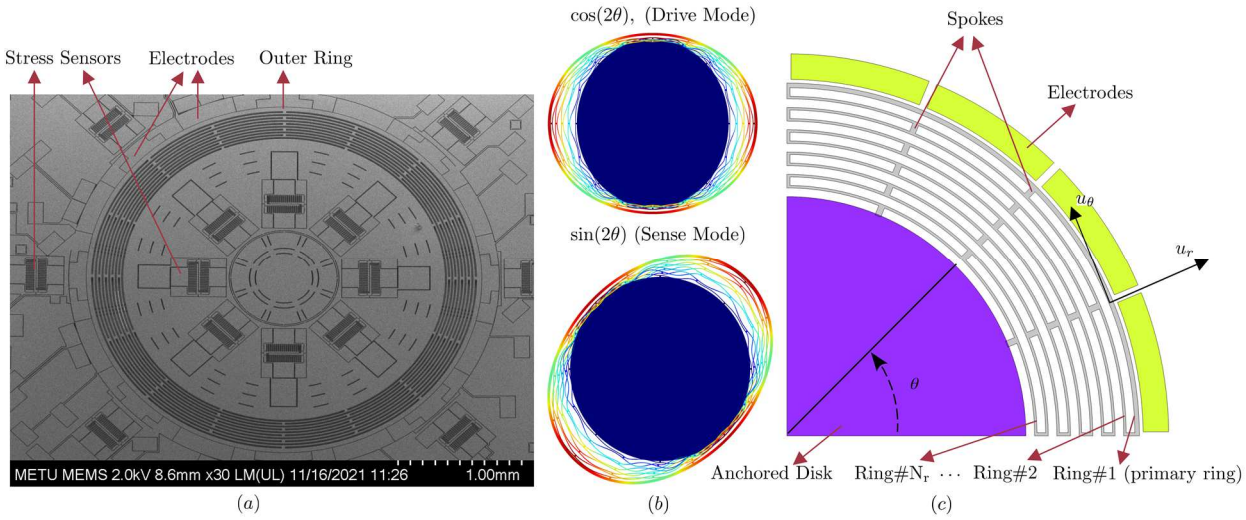


(a) (b) (c)

*Figure 1. (a) SEM image of the fabricated DRG, (b) operating mode shapes, and (c) schematics of the DRG.*

*Table 1: Parameters of fabricated DRG.*

| **Parameter** | Number of rings ($N_r$) | Mean radius of Ring#1 ($R_1$) | Width of Ring#1 ($w_1$) | Average width of Rings#2-10* | Spoke length ($\ell$) | Spoke width | Thickness |
|---|---|---|---|---|---|---|---|
| **Value** | 10 | 1699 μm | 41μm | 11.44 μm | 17.5 μm | 40 μm | 35 μm |

*We have a varying width design for the suspension rings.

of two separate rotations [9]: 1) caused by the radial displacement's gradient, 2) caused by the tangential motion. Mathematically,

$$u_{\theta,i+1}(\theta_{i,j},t) - \frac{\ell}{R_{i+1}}\left(\frac{\partial u_{r,i+1}(\theta,t)}{\partial\theta}\,|_{\theta_{i,j}} - u_{\theta,i+1}(\theta_{i,j},t)\right) = u_{\theta,i}(\theta_{i,j},t), i = 1{:}\,N_r-1, j = 1{:}\,4n, \quad u_{\theta,N_r}(\theta_{N_r,j},t) = 0, j = 1{:}\,4n. \tag{3}$$

**Basis functions for mode shapes**

As a result of rings' circular symmetry, their mode shapes occur in the form of degenerate pairs with a single natural frequency. Combining this property with the inextensibility of the rings' centerlines, for the $n$-th mode we have

$$u_{\theta,i}(\theta,t) = -Q_1(t)\int_0^\theta f_i(\tau;n)\mathrm{d}\tau - Q_2(t)\int_0^\theta g_i(\tau;n)\mathrm{d}\tau\,, \quad u_{r,i}(\theta,t) = Q_1(t)f_i(\theta;n) + Q_2(t)g_i(\theta;n), \tag{4}$$

where the mode shapes $f_i(.), g_i(.) \in \mathbb{R}$ are (at least) $2\pi$-periodic continuous functions that satisfy the orthogonality condition $\int_0^{2\pi} f_i(\theta;n)g_i(\theta;n)\,\mathrm{d}\theta = 0$, and $Q_1(.) \in \mathbb{R}$ and $Q_2(.) \in \mathbb{R}$ are the generalized coordinates associated with the displacements of $f_i(.)$ and $g_i(.)$, respectively. We assume that the suspension system is compliant enough so that it does not significantly distort the modal space of Ring#1 in its free standing case. Accordingly, the $n$-th mode shapes of Ring#1 are (see Figure 1-(b))

$$f_1(\theta;n) = \cos(n\theta)\,, g_1(\theta;n) = \sin(n\theta). \tag{5}$$

Now, our objective is to calculate the mode shapes of Rings#2: $N_r$, given the mode shapes (5) of Ring#1. For this, we consider the suspension as a linear system (because gyroscope's operation range is in the Si's linear elastic region) subjected to $f_1(\theta;n)$ and $g_1(\theta;n)$ as its inputs. On this basis, we proceed with the following observations:

1. The suspension system, due to its linearity, preserves the period of its inputs, and therefore, $f_i(\theta;n)$ and $g_i(\theta;n)$ are $\frac{2\pi}{n}$-periodic. Moreover, $f_i(\theta;n)$ and $g_i(\theta;n)$ will have the same relative phase shift of $\frac{\pi}{2n}$ as $f_1(\theta;n)$ and $g_1(\theta;n)$. This means that we only need to calculate the responses $f_i(\theta;n)$ to $f_1(\theta;n)$ and $g_i$'s can be obtained as $g_i(\theta;n) = f_i(\theta - \frac{\pi}{2n};n)$, $i = 2{:}\,N_r$.
2. A careful inspection reveals that the suspension system preserves the evenness of $f_1(\theta;n)$ and—same as $f_1(\theta;n)$ —has a pair of consecutive maximum-minimum at the angles 0 and $\pi/2n$.

These two observations give us $\{\cos((2j-1)n\theta) : j = 1,2,\cdots\}$ as the underlying set of basis functions for the mode shapes $f_i(\theta;n)$. Accordingly, we form the truncated expansions

$$f_i(\theta;n) \approx \phi^\top(\theta;n)\alpha_i, i = 2{:}\,N_r, \tag{6}$$

where $\phi(\theta;n) = \left[\cos(n\theta)\,,\cos(3n\theta)\,,\ldots,\cos\big((2N-1)n\theta\big)\right]^\top \in \mathbb{R}^N$ is the vector of basis functions and $\alpha_i \in \mathbb{R}^N$ is the vector of their coefficients; $N$ is the number of basis of functions that we use to approximate the mode shapes. Let $\varphi(\theta;n) \coloneqq \int_0^\theta \phi(\theta;n)\mathrm{d}\tau$; the basis functions satisfy the following properties over the spoke angles:

1. If ring number $i$ is odd:

$$\phi(\theta_{i,j};n) = \begin{cases} 0, & \text{if } j \text{ is even,} \\ (-1)^{\frac{j-1}{2}}\phi(\theta_{i,1};n), & \text{if } j \text{ is odd,} \end{cases}$$
$$\phi'(\theta_{i,j};n) = \begin{cases} (-1)^{\frac{j}{2}-1}\phi'(\theta_{i,2};n), & \text{if } j \text{ is even,} \\ 0, & \text{if } j \text{ is odd,} \end{cases} \tag{7}$$
$$\varphi(\theta_{i,j};n) = \begin{cases} (-1)^{\frac{j}{2}-1}\varphi(\theta_{i,2};n), & \text{if } j \text{ is even,} \\ 0, & \text{if } j \text{ is odd,} \end{cases}$$

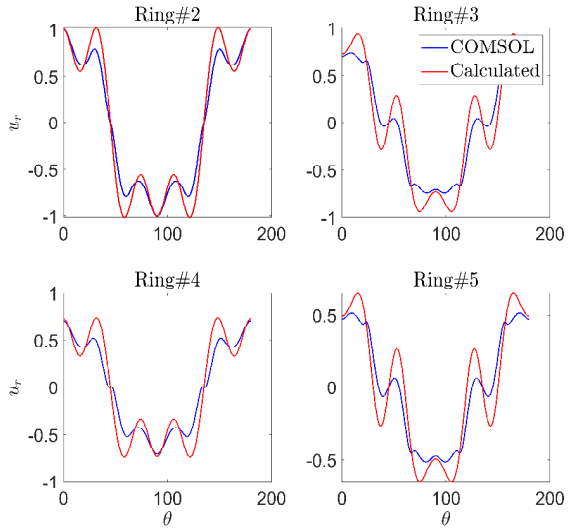


*Figure 2. Calculated and FEM mode shapes of Rings#2-5*

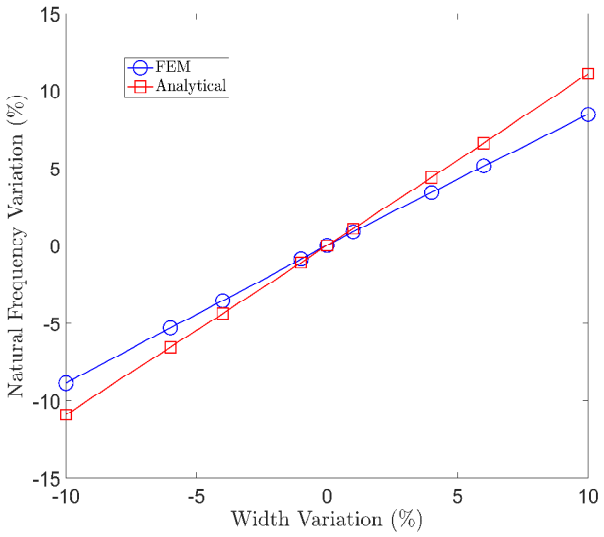


*Figure 3. Variations of calculated natural frequencies versus width variation of rings*

2. If ring number $i$ is even:

$$\phi(\theta_{i,j};n)=\begin{cases}\phi(\theta_{i,1};n),\text{if } j\equiv 0,1 \pmod 4,\\ -\phi(\theta_{i,1};n),\text{if } j\equiv 2,3 \pmod 4,\end{cases}$$
$$\phi'(\theta_{i,j};n)=\begin{cases}\phi'(\theta_{i,2};n),\text{if } j\equiv 1,2 \pmod 4,\\ -\phi'(\theta_{i,2};n),\text{if } j\equiv 0,3 \pmod 4,\end{cases} \quad (8)$$
$$\varphi(\theta_{i,j};n)=\begin{cases}\varphi(\theta_{i,2};n),\text{if } j\equiv 1,2 \pmod 4,\\ -\varphi(\theta_{i,2};n),\text{if } j\equiv 0,3 \pmod 4.\end{cases}$$

In view of the properties (7) and (8), expansion (6) allows us to simplify the $8nN_r$ equations in the boundary conditions (2) and (3) to the following set of $2N_r$ equations:

$$\begin{aligned}&\phi^{\top}(\theta_{1,1};n)\alpha_2=\cos(n\theta_{1,1}),\\ &\phi^{\top}(\theta_{i,1};n)(\alpha_{i+1}-\alpha_i)=0, i=2{:}\,N_r-1,\\ &\phi^{\top}(\theta_{N_r,1};n)\alpha_{N_r}=0,\\ &\left(\left(1+\frac{\ell}{R_2}\right)\varphi^{\top}(\theta_{1,2};n)+\frac{\ell}{R_2}\phi'^{\top}(\theta_{1,2};n)\right)\alpha_2\\ &=\frac{\sin(n\theta_{1,2})}{n},\\ &\left(\left(1+\frac{\ell}{R_{i+1}}\right)\varphi^{\top}(\theta_{i,2};n)+\frac{\ell}{R_{i+1}}\phi'^{\top}(\theta_{i,2};n)\right)\alpha_{i+1}\\ &-\varphi^{\top}(\theta_{i,2};n)\alpha_i=0, i=2{:}\,N_r-1,\\ &\varphi^{\top}(\theta_{N_r,2};n)\alpha_{N_r}=0.\end{aligned} \quad (9)$$

Defining $\alpha\coloneqq[\alpha_2^{\top},\cdots,\alpha_{N_r}^{\top}]^{\top}\in\mathbb{R}^{N(N_r-1)}$ as the augmented vector of unknown coefficients, we put the equations in (9) into the following matrix form:

$$A\alpha=b, \quad (10)$$

where $A\in\mathbb{R}^{2N_r\times N(N_r-1)}$ and $b\in\mathbb{R}^{2N_r}$.

## Calculating mode shapes

The Ritz method stipulates that the mode shapes of a mechanical structure extremize its total potential energy subject to the boundary conditions [10]. In our case, the total potential energy is the strain energy stored in the suspension rings due to the $n$-th mode shapes, and it is given by

$$\mathcal{V}_{susp}=\sum_{i=2}^{N_r}\frac{EI_i}{2R_i^3}\int_0^{2\pi}\left(f_i(\theta;n)+f_i''(\theta;n)\right)^2\mathrm{d}\theta, \quad (11)$$

where $E$ is Young's modulus. By substituting the expansion (6) into (11), we reduce the Ritz method to the following least-squares optimization problem:

$$\begin{aligned}&\alpha^*=\arg\min_{\alpha} V_{susp}\approx\frac{1}{2}\alpha^{\top}P_k\alpha\\ &\text{subject to}\\ &A\alpha=b,\end{aligned} \quad (12)$$

where $\alpha^*\in\mathbb{R}^N$ is the optimal coefficients' vector and

$$\begin{aligned}&P_k=\mathrm{diag}\left(\frac{EI_i}{R_i^3}\right)_{i=2}^{N_r}\otimes\Pi_k,\\ &\Pi_k\\ &=\int_0^{2\pi}(\phi(\theta;n)+\phi''(\theta;n))(\phi(\theta;n)+\phi''(\theta;n))^{\top}\mathrm{d}\theta\\ &=\pi\mathrm{diag}((1-(2j-1)^2n^2)^2)_{j=1}^{N}.\end{aligned} \quad (13)$$

To ensure that we not only satisfy the boundary conditions but also minimize the potential function, we select the number of basis functions such that $N>\left[\frac{2N_r}{N_r-1}\right]$ to render the system (10) underdetermined. Problem (12) can be solved accurately and efficiently using MATLAB's `lsqr` command.

## Modal properties

After obtaining $\alpha^*$, we calculate the modal properties:

- Effective mass:

$$\begin{aligned}&m=\sum_{i=1}^{N_r}\rho R_iA_i\int_0^{2\pi}f^2(\theta;n)+\left(\int_0^{\theta}f_i(\tau;n)\mathrm{d}\tau\right)^2\mathrm{d}\theta\\ &=\pi\rho R_1A_1\left(\frac{n^2+1}{n^2}\right)+\alpha^{*\top}P_m\alpha^*,\\ &P_m=\mathrm{diag}(\rho R_iA_i)_{i=2}^{N_r}\otimes\Pi_m,\\ &\Pi_m=\int_0^{2\pi}\phi(\theta;n)\phi^{\top}(\theta;n)+\varphi(\theta;n)\varphi^{\top}(\theta;n)\mathrm{d}\theta\\ &=\pi\mathrm{diag}\left(1+\frac{1}{(2j-1)^2n^2}\right)_{j=1}^{N}.\end{aligned} \quad (14)$$

- Coriolis mass:

$$m_c = \sum_{i=1}^{N_r} \rho R_i A_i \int_0^{2\pi} \int_0^{\theta} f_i(\tau;n)\, g_i(\theta;n) - f_i(\theta;n) g_i(\tau;n) \mathrm{d}\tau \mathrm{d}\theta = \frac{2\pi\rho R_1 A_1}{n} + \alpha^{*\top} P_c \alpha^*,$$
$$P_c = \mathrm{diag}(\rho R_i A_i)_{i=2}^{N_r} \otimes \Pi_c, \quad (15)$$
$$\Pi_c = \int_0^{2\pi} \varphi(\theta;n)\phi^{\top}\left(\theta - \frac{\pi}{2n};n\right) - \phi(\theta;n)\varphi^{\top}\left(\theta - \frac{\pi}{2n};n\right) \mathrm{d}\theta = \frac{2\pi}{n}\mathrm{diag}\left(\frac{(-1)^{j+1}}{2j-1}\right)_{j=1}^{N}.$$

- Effective stiffness:

$$k = \sum_{i=1}^{N_r} \frac{EI_i}{R_i^3} \int_0^{2\pi} \left(f_i(\theta;n) + f_i''(\theta;n)\right)^2 \mathrm{d}\theta = \frac{\pi E I_1}{R_1^3}(n^2-1)^2 + \alpha^{*\top} P_k \alpha^*. \quad (16)$$

The derivation of the above equations can be found in [4]. The natural frequency of the $n$-th mode is $\omega_n = \sqrt{k/m}$, and its angular gain [11] is $A_g = \frac{m_c}{nm}$ that quantifies the device's structural efficacy in Coriolis-based energy transfer from the drive to the sense mode.

## RESULTS

The key parameters of our DRG are given in Table 1. We measured its resonance frequencies and quality factors as 41.173 kHz, 50.57k for the drive mode ($\cos(2\theta)$) and 41.159 kHz, 45.56k for the sense mode ($\sin(2\theta)$); there is a 14 Hz frequency split between the modes, which is attributable to geometric imperfections. We implemented our method in MATLAB. As a reference for comparison, we also performed FEM-based modal analysis in COMSOL Multiphysics that gave us the natural frequency 45.216 kHz. With $N = 3$ basis functions, the comparative graphs of our calculated and FEM mode shapes are given in Figure 2. At the spoke angles, the two mode shapes match very closely; however, our calculated mode shapes exhibit larger amplitudes at the other angles,. We obtained the modal properties as $m = 4.765 \times 10^{-8}$ kg, $m_c = 3.545 \times 10^{-8}$ kg, and $k = 3.339 \times 10^{3}$ N/m; these values give us the natural frequency as 42.134 kHz, which has the relative errors of 2.4% and 6.8% with respect to the experimental and FEM values, respectively. The mismatch between our results and FEM is due to neglected strain energies of the spokes and variations of the displacement fields across rings. Furthermore, based on the mismatch between calculated and measured frequencies, we estimate that a 200 nm mask bias has occurred in the lithography. We also obtain the angular gain of our gyroscope as 0.3723, which is 7% less than the theoretical value of 0.4 for a single ring. This observation points out the limiting effect of the suspension system on the angular gain of circular gyroscopes. Figure 3 shows the comparative graphs of natural frequency variation against the width variation of our method and FEM; we observe a linear pattern in both methods, which guarantees the consistency of our modeling.

## CONCLUSION

We demonstrated a new method to calculate the mode shapes and modal properties of DRGs. By introducing an accurate numerical integration scheme, our method can be extended to model the effects of geometrical imperfections caused, for example, by nonuniform etching as well as Young's modulus anisotropy, which is well known to exist in (100) Si wafers. Such an approach can provide an analytical framework to study frequency split and quadrature error in DRGs.

## ACKNOWLEDGEMENTS

This work was supported by the Scientific and Technological Research Council of Turkey (TUBITAK) 2232 Program with the grant number 118C247. The ideas/claims presented here solely belong to authors.

## REFERENCES

[1] P. Taheri-Tehrani *et al.*, "Disk resonator gyroscope with whole-angle mode operation," *Inertial 2015*, Mar. 2015, pp. 1–4.

[2] Q. Li *et al.*, "0.04 degree-per-hour MEMS disk resonator gyroscope with high-quality factor (510 k) and long decaying time constant (74.9 s)," *Microsyst. Nanoeng.*, vol. 4, no. 1, pp. 1–11, Nov. 2018.

[3] Y. Xu *et al.*, "0.015 Degree-Per-Hour Honeycomb Disk Resonator Gyroscope," *IEEE Sens. J.*, vol. 21, no. 6, pp. 7326–7338, Mar. 2021.

[4] M. Hosseini-Pishrobat and E. Tatar, "Analysis of Quadrature and Frequency Split in a MEMS Vibrating Ring Gyroscope with Structural Imperfections," *Transducers 2021* (Virtual Conference), Jun. 2021, pp. 1291–1294.

[5] S. W. Yoon, S. Lee, and K. Najafi, "Vibration sensitivity analysis of MEMS vibratory ring gyroscopes," *Sens. Actuators Phys.*, vol. 171, no. 2, pp. 163–177, Nov. 2011.

[6] Q. Li *et al.*, "Dynamic Modeling of the Multiring Disk Resonator Gyroscope," *Micromachines*, vol. 10, no. 3, Art. no. 3, Mar. 2019.

[7] C. Lin, J. Zhao, Z. Yao, Q. Fan, B. Mo, and Y. Su, "Vibration modeling of disk resonator gyroscope by wave propagation," *J. Sound Vib.*, vol. 444, pp. 85–107, Mar. 2019.

[8] M. M. Torunbalci, S. E. Alper, and T. Akin, "Advanced MEMS Process for Wafer Level Hermetic Encapsulation of MEMS Devices Using SOI Cap Wafers With Vertical Feedthroughs," *J. Microelectromechanical Syst.*, vol. 24, no. 3, pp. 556–564, Jun. 2015.

[9] S. J. Walsh and R. G. White, "Vibrational Power Transmission in Curved Beams," *J. Sound Vib.*, vol. 233, no. 3, pp. 455–488, Jun. 2000.

[10] C. L. Dym and I. H. Shames, *Solid Mechanics: A Variational Approach*, Augmented Edition. New York, NY: Springer New York, 2013.

[11] M. W. Putty, "A micromachined vibrating ring gyroscope," Ph.D. Dissertation, University of Michigan, 1995.

## CONTACT

*M. Hosseini-Pishrobat, Tel: +90-312-2901219; mehran@ee.bilkent.edu.tr